Discretising Barrick's equations

By J. J. Green

Dept. Applied Mathematics, University of Sheffield, UK

1. Introduction

The use of the Doppler spectrum of HF radar backscatter for the remote sensing of the ocean's surface is now well-established, with a large literature and numerous deployments for commercial and scientific applications. Part of the attraction is the versatility of the technology: ocean currents can be monitored over a large coastal area with relatively inexpensive radars and small computational cost; the same signal can be used to estimate high-frequency ocean waves, and so the strength and direction of prevailing winds. The theoretical extraction of the full directional spectrum of ocean waves from HF backscatter, first established by Barrick in the 1970s, has been slower to develop due to its need for high quality measured backscatter and substantial computational resources, barriers that have all but disappeared in recent years.

In this article we describe a general discretisation scheme for Barrick's equations based on the observation that the linearised equations can be viewed as a local weighted projection transform, and demonstrate that techniques from the global unweighted case, in particular from transmission tomography, can be applied quite naturally. The generality of the discretisation allows it to be applied to a number of inversion algorithms, and we demonstrate implementation with the popular tomographic inversion algorithm ART, which we find able to perform real-time inversion of measured backscatter on modest hardware.

2. Background

In this section we give a brief overview of Barrick's equations modelling the Doppler spectrum of HF (high frequency) radar echos from the sea's surface. Readers seeking the derivation of these are referred to the articles of Barrick (1972), Weber & Barrick (1977), Barrick & Weber (1977), and to the more recent expositions of Holden & Wyatt (1992) and Hisaki (1996).

In the interests of notational brevity we will treat the version of Barrick's equations for water of infinite depth — the extension to the shallow water case is straightforward.

Barrick's equations

Barrick's equations relate σ, the Doppler spectrum of the backscattered radar signal, to S, the ocean wavenumber spectrum in the absence of current. The equations are derived by a perturbation analysis leading to an expansion $\sigma = \sigma_1 + \sigma_2 + \cdots$, whose first term is given by

$$\sigma_1(\omega, \phi) = 2^6 \pi k_0^4 \sum_{m=\pm 1} S(-m\mathbf{k}_0)\delta(\omega - m\omega_\mathrm{b}), \tag{2.1}$$

where ω is the angular frequency of the Doppler shift, $\mathbf{k}_0$ the wavevector of the incident HF radar beam with wavenumber k_0 and direction ϕ, S the ocean wavevector spectrum and

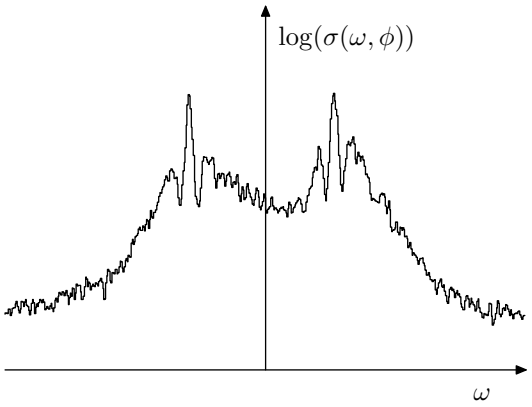

FIGURE 1. An example of measured Doppler spectra

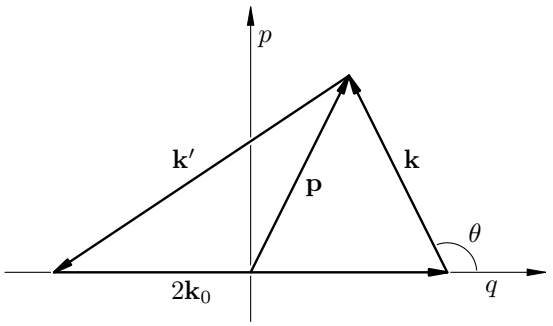

FIGURE 2. Geometry of the wavevectors at second order

ω_b the frequency of the Bragg matched waves, given by the linear dispersion relationship

$$\omega_\mathrm{b} = \sqrt{2gk_0}.$$

The distributional equation (2.1) defines impulses in the Doppler spectrum σ at $\pm\omega_\mathrm{b}$, features which can clearly be identified in measured spectra, for example in Figure 1.

The second order term, σ_2, derived in the series of papers by Barrick *et al.* mentioned above, may be written

$$\sigma_2(\omega,\phi) = 2^6\pi k_0^4 \sum_{m,\,m'=\pm1} \int_{\mathbf{R}^2} |\Gamma|^2 \, S(m\mathbf{k})S(m'\mathbf{k}')\delta(\omega - m\sqrt{gk} - m'\sqrt{gk'})\,\mathrm{d}\mathbf{p}. \quad (2.2)$$

Here the wave vectors $\mathbf{k}$ and $\mathbf{k}'$ satisfy the Bragg resonance condition $\mathbf{k}+\mathbf{k}' = -2\mathbf{k}_0$, and are related to the variable of integration $\mathbf{p}$ by

$$\mathbf{k}+\mathbf{k}_0 = \mathbf{p}, \quad \mathbf{k}'+\mathbf{k}_0 = -\mathbf{p}$$

as is illustrated in Figure 2.

The kernel $|\Gamma|^2$ in (2.2) is determined by the *coupling coefficient*,

$$\Gamma = \Gamma(\omega, k, \theta, mm'),$$

which is the sum of contributions accounting for nonlinear hydrodynamic effects (direct backscatter from second-order, Stokes, waves) and for nonlinear electromagnetic effects (indirect backscatter from pairs of first-order waves). The reader is referred to Weber & Barrick (1977), Barrick & Weber (1977) and Barrick & Lipa (1986) for details on the kernel, as we will only need the fact that it is symmetric about the natural coordinate axes of the integration variable $\mathbf{p} = (p, q)$ illustrated in Figure 2.

It is convenient to write Barrick's equations in terms of the dimensionless variables

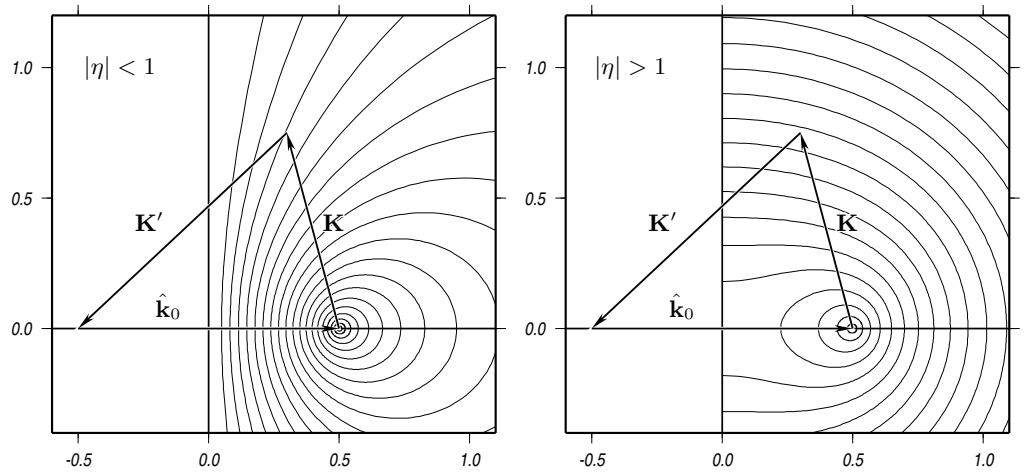

FIGURE 3. Integration curves for the normalised second-order equation

$\eta = \omega/\omega_\mathrm{b}$, $\mathbf{K} = \mathbf{k}/2k_0$, $\mathbf{K}' = \mathbf{k}'/2k_0$. The normalised directional spectrum $Z = S/(2k_0)^4$ is then related to the normalised Doppler spectrum $\sigma(\eta, \phi) \equiv \omega_\mathrm{b}\sigma(\omega, \phi)$ to first order by

$$\sigma_1(\eta, \phi) = \sum_{m=\pm 1} Z(-2m\hat{\mathbf{k}}_0)\delta(\eta - m) \tag{2.3}$$

where $\hat{\mathbf{k}}_0 = \mathbf{k}_0/k_0$, and to second order by

$$\sigma_2(\eta, \phi) = 8\pi \sum_{m,\, m'=\pm 1} \int_{\mathbf{R}^2} |\Gamma|^2 \, Z(m\mathbf{K})Z(m'\mathbf{K}')\delta(\eta - m\sqrt{K} - m'\sqrt{K'}) \, \mathrm{d}\mathbf{p}. \tag{2.4}$$

For each Doppler frequency $|\eta| < 1$, the Dirac constraint ensures that there are exactly two nonzero summands in (2.4), integrals over a curves which are reflections in the q-axis. On the other hand, for $|\eta| > 1$ there is only one nonzero summand in (2.4), and this is an integral over a curve (or curves, for $1 < |\eta| < \sqrt{2}$) symmetric about the q-axis. It follows that we can write (2.4) as

$$\sigma_2(\eta, \phi) = 16\pi \int_{K<K'} |\Gamma|^2 \, Z(m\mathbf{K})Z(m'\mathbf{K}')\delta(|\eta| - m\sqrt{K} - m'\sqrt{K'}) \, \mathrm{d}\mathbf{p}. \tag{2.5}$$

where m and m' depend on η,

$$m = \begin{cases} 1 & \eta > 0 \\ -1 & \eta < 0 \end{cases}, \qquad m' = \begin{cases} 1 & |\eta| < 1 \\ -1 & |\eta| > 1 \end{cases}.$$

The curves of integration in (2.5) are illustrated in Figure 3.

Linearisation

The inversion of equation (2.5), i. e., finding the directional spectrum Z from Doppler spectral data σ, is complicated by nonlinearity. Fortunately the inversion is particularly amenable to linearisation in practice — for radars of suitable frequency the larger wave vector $\mathbf{K}'$ corresponds to higher frequency ocean waves which quickly align to prevailing winds, and whose directional spectrum is well approximated by empirical models such as Pierson & Moskowitz (1964). Indeed, it is practical to fit such a model to the ocean spectral data provided by the inversion of the first-order equation (2.1), i. e., from the Bragg peaks. See, for example, the discussion in Wyatt, Ledgard & Anderson (1997).

Writing $G = G(\mathbf{K})$ for the estimate of the directional spectrum obtained from such a model, solving (2.5) for the Dirac constraint and making θ, the direction of $\mathbf{K}$ relative to $\mathbf{k}_0$ (as in Figure 2), the variable of integration, we obtain the linear approximation

$$\sigma(\eta, \phi) = \int_{-\pi}^{\pi} \Lambda(\mathbf{K}, \phi) Z(m\mathbf{K}) \, \mathrm{d}\theta \tag{2.6}$$

where the kernel Λ has absorbed that in (2.5), the model estimate of $Z(m'\mathbf{K}')$, the Jacobian of the change of integration variable and the integration constraint

$$\Lambda = \begin{cases} 16\pi \left|\Gamma\right|^2 G(m'\mathbf{K}') \frac{\partial|\omega|}{\partial K} & K < K' \\ 0 & \text{otherwise} \end{cases}.$$

We henceforth consider only the linearised equation (2.6), but much of what is described below could be extended to work with the fully nonlinear equation, albeit with additional computational and notational complexity.

Availability of data

Although the equations (2.3) and (2.6) provide rather good agreement with measured HF radar backscatter, there are a number of limitations on the measurement of Doppler spectra which should be borne in mind when attempting the inversion of (2.6) with real data.

In measured backscatter, e. g., Figure 1, the Bragg peaks, although evident, are smeared in (Doppler) frequency. Such effects could be caused by variation in the ocean current in the observed area, or by the measurement of the signal with (necessarily) band-limited equipment. This leads to a problem, yet to be satisfactorily solved, in determining which part of the signal is first-order, and which second. In practice this leads to a bound on the quantity $|\eta| - 1$ for second order data σ, corresponding to a lower bound on K in the directional spectrum Z.

The inevitable presence of noise in the measured signal is also apparent in Figure 1, since for any physically reasonable exact data Z we would expect σ to be a smooth function of η, barring ± 1, decaying rapidly with increasing η and as $\eta \to \pm 1$. Thus measured data with reasonable signal to noise ratio is restricted to Doppler frequencies for which $||\eta| - 1|$ is in some positive interval, and so restricts the wavenumbers K at which we can reconstruct the directional spectrum Z.

Finally, radars capable of measuring second-order Doppler spectra to the accuracy required for inversion are rather expensive. Two radars are needed to resolve left-right ambiguities, but for purely economic reasons an inversion technique requiring more than two would find limited application.

3. Discretisation for inversion

The problem of inverting Barrick's equation (2.4) is that of recovering a function from integrals over curves in its domain. In this respect the problem is one of *integral geometry*, who's most studied special case is the inversion of the x-ray and Radon transforms (which are the same in two dimensions). See, for example, Helgason (1999). Such inversions arise in a number of problems in image processing, electron microscopy, astronomy, and in particular, medical and process tomography. The reader is referred to Natterer & Wübbeling (2001) for an extensive overview of this field and its literature.

One popular method for inversion of the x-ray transform is to evaluate numerically the inversion formula derived by Radon in 1937 (see §5.1 of Natterer & Wübbeling (2001)).

This allows the expression of the problem in terms of the Fourier transform, allowing solution by fast Fourier methods. Such techniques, however, depend rather delicately on the geometry of the lines along which integrals are taken, and so would seem difficult to extend to more general curves.

Another widely studied approach for these problems relies on the fact that they can be sparsely discretised. If the unknown function is represented by a basis of functions with small support (for example the characteristic functions of a grid of pixels), then each line over the function's domain will intersect only a few of the supports. The resultant sparse discretisations can then be solved efficiently for the coefficients, often by iterative row-action methods as described by Censor (1981). For a discretised problem $y = Ax$ and initial estimate $x^{(0)}$ one obtains iteratively improved estimates $x^{(i+1)}$ from the calculated value of $A_j x^{(i)}$ and y_j, where A_j is the jth row of A and the index j cycles through the row-indices of A.

The seminal example of a row-action method, discovered by Kaczmarz in 1917, is the algebraic reconstruction technique (ART), (see Gordon, Bender & Hermann (1970)) implemented by Hounsfield in the EMI computerised tomography scanner (see Hounsfield (1973)). For the ART, the iterative step is

$$x^{i+1} \leftarrow x^i + \lambda \frac{(y_j - A_j x^{(i)})}{\|A_j\|_2^2} A_j^{\mathrm{T}}$$

where $\lambda \in (0, 2)$ is the relaxation parameter. For $\lambda = 1$ each step of the ART is the projection of $x^{(i)}$ onto the hyperplane defined by jth row of the problem, $A_j x = y_j$.

The ART and its many variants are, of course, easy to implement in a manner which exploits sparsity, and in tomographic applications surprisingly few iterations are needed, typically 4–15 cycles through the rows of the matrix (Matej *et al.* (1994)). Indeed, it is shown in Flemming (1980) that early termination of the ART regularises (in the sense of Tikhonov) the ill-posed nature of the problem that has been discretised.

In the remainder of this note we discuss the discretisation of Barrick's equation for inversion by such row-action methods.

Barrick's equation

Suppose that the normalised directional spectrum Z in Barrick's linearised second order equation (2.6) is to be represented as a linear combination of basis functions b_i,

$$Z(\mathbf{K}) = \sum_i \xi_i b_i(\mathbf{K}). \tag{3.1}$$

Seeking a sparse but general discretisation, we initially assume only that each b_i has a small support. Measured Doppler spectra are typically available as binned data,

$$\sigma_j = \frac{1}{\eta_{j+1} - \eta_j} \int_{\eta_j}^{\eta_{j+1}} \sigma(\eta)\, \mathrm{d}\eta, \tag{3.2}$$

where $\Delta\eta \equiv \eta_{j+1} - \eta_j$ is henceforth assumed constant. Thus each inversion datum σ_j corresponds to a *strip* integral in the wavevector domain of Z. Since these strips narrow quadratically as η_j approaches ± 1, the representation in (3.1) should scale similarly if it seeks to discretise uniformly with respect to the measured data. This scaling is absorbed into the problem by introducing the variable $\mathbf{y}$, the vector of length $\sqrt{K}$ in the direction of $\mathbf{K}$, so that (2.6) becomes

$$\sigma(\eta, \phi) = \int_{-\pi}^{\pi} \Lambda(\mathbf{y}, \phi) Z(m\mathbf{y})\, \mathrm{d}\theta \tag{3.3}$$

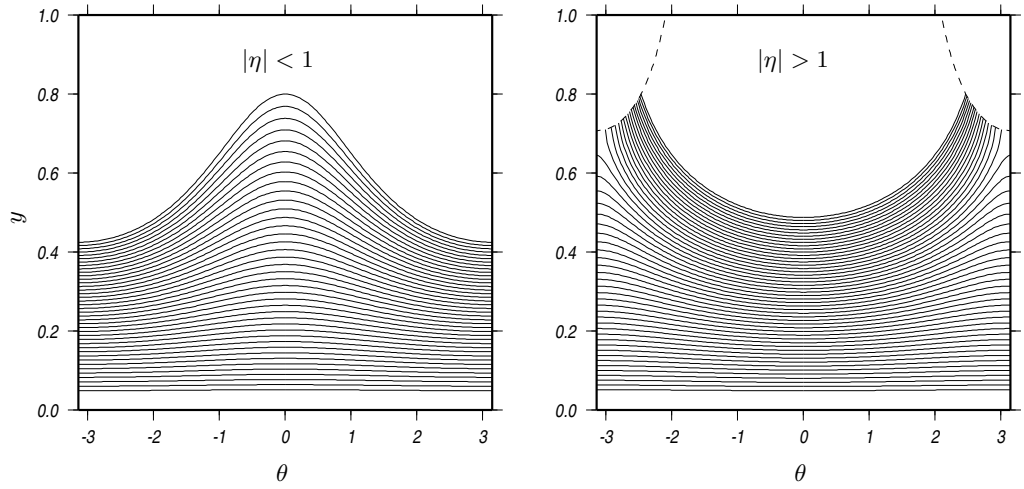

FIGURE 4. Integration curves for the normalised second-order equation. Points $\mathbf{y} = (y, \theta)$ above the dashed line correspond to normalised wave-vectors $\mathbf{K}$ with $\mathbf{K} > \mathbf{K}'$.

where

$$\Lambda = \begin{cases} 16\pi \left|\Gamma\right|^2 G(m'\mathbf{K}') \frac{\partial|\omega|}{\partial K} \frac{\partial K}{\partial y} & K < K' \\ 0 & \text{otherwise} \end{cases}$$

has absorbed the Jacobian of the transformation. The integration curves in the y-θ domain are illustrated in Figure 4.

Combining the representations (3.1) and (3.2) with the formulation of Barrick's equation in the $\mathbf{y}$ domain gives

$$\sigma_j = \sum_i \frac{1}{\Delta\eta} \xi_i \int_{\eta_j}^{\eta_{j+1}} \int_{-\pi}^{\pi} \Lambda(\mathbf{y}, \psi) b_i(m\mathbf{y}) \, \mathrm{d}\theta \, \mathrm{d}\eta. \tag{3.4}$$

Taking $\mathbf{y}_i$ to be some point in the support of b_i, and supposing that this support is so small that Λ is well approximated on it by $\Lambda_i \equiv \Lambda(\mathbf{y}_i)$, we find that (3.4) reduces to the linear system

$$\sigma_j = \frac{1}{\Delta\eta} \sum_i \Lambda_i B_{i,j} \xi_i, \tag{3.5}$$

where

$$B_{i,j} \equiv \int_{\eta_j}^{\eta_{j+1}} \int_{-\pi}^{\pi} b_i(m\mathbf{y}) \, \mathrm{d}\theta \, \mathrm{d}\eta \tag{3.6}$$

is the jth strip integral over the ith basis function. Writing C_j for the strip

$$\{\mathbf{y}(\eta, \theta) : \eta_j \le \eta \le \eta_{j+1}\}$$

we have

$$B_{i,j} = \int_{C_j} b_i(m\mathbf{y}) \frac{\partial \eta}{\partial y}(m\mathbf{y}) \, \mathrm{d}\mathbf{y} \approx \frac{\partial \eta}{\partial y}(m\mathbf{y}_i) \int_{C_j} b_i(m\mathbf{y}) \, \mathrm{d}\mathbf{y} \tag{3.7}$$

provided, again, that the support of b_i is sufficiently small.

The final integral in (3.7) can be evaluated approximately by introducing orthogonal coordinates (s, t), based at $\mathbf{y}_i$ and with s in the direction of increasing η. Then by Taylor

$$\eta(s, t) \approx \eta(\mathbf{y}_i) + \left|\nabla\eta(\mathbf{y}_i)\right| s \tag{3.8}$$

so that

$$\int_{C_j} b_i(m\mathbf{y})\,\mathrm{d}\mathbf{y} \approx \int_{s_{i,j}}^{s_{i,j+1}} \int_{-t_i}^{t_i} b_i(m\mathbf{y}(s,t))\,\mathrm{d}s\,\mathrm{d}t, \tag{3.9}$$

where the t_i are chosen so that all points (s,t) in the support of b_i have $-t_i < t < t_i$ and where, from (3.8), the

$$s_{i,j} = \frac{\eta_j - \eta(\mathbf{y}_i)}{|\nabla\eta(\mathbf{y}_i)|} \tag{3.10}$$

are the limits of integration of the *projection* of the basis function b_i in the direction of the coordinate t. The point of the approximation of a curved strip integral by a projection, as illustrated in Figure 5, is that for a suitable choice of basis function b_i, projections can be calculated explicity.

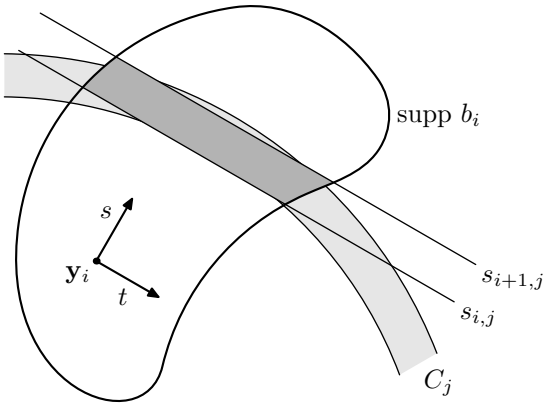

FIGURE 5. Geometry of the strip integral approximation

For completeness, we mention that the partial derivatives in (3.7) and (3.8), conveniently written with the dual variable $\mathbf{y}'$ in the direction of $\mathbf{K}'$ and of length $y' = \sqrt{K'}$, are

$$\frac{\partial\eta}{\partial y} = mF(y,D) + m'\frac{y(y^2+\cos\theta)}{(y')^3}F(y',D), \qquad \frac{\partial\eta}{\partial\theta} = -m'\frac{y^2\sin\theta}{2(y')^3}F(y',D) \tag{3.11}$$

with the dependence on the normalised water depth $D \equiv d/2k_0$ given by

$$F(y,D) = (1 + 2y^2D\operatorname{cosech}2y^2D)\sqrt{\frac{\tanh y^2D}{\tanh D}},$$

which can taken as 1 in the deep water case.

Basis functions

The strip integral approximation (3.7) aims to treat the transformation defined by Barrick's equation (3.4) as being, locally, a weighted projection transform. This approach makes available the store of techniques and results on projection transforms, provided they are amenable to localisation. In this section we discuss the recent research of Lewitt and co-workers on functional representation for projection transforms (Lewitt (1990), Matej *et al.* (1994), Matej (1996)) and describe how these can be applied to Barrick's equation in a straightforward manner.

Lewitt has observed that, in a representation of a function by a linear combination of basis functions, it is desirable that the basis be effectively band-limited, i. e., that the Fourier transforms of the basis functions be localised around zero, since this imposes constraints on the smoothness of the function so represented (Lewitt (1990)). For an

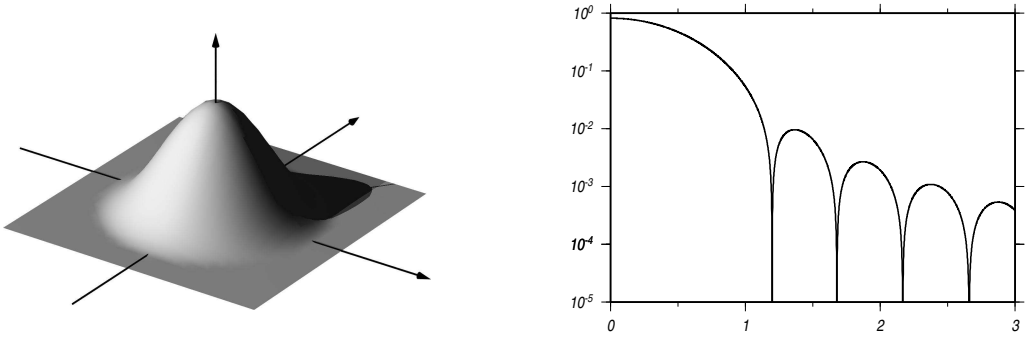

FIGURE 6. Lewitt's basis function Ψ for $m = 2$, $\alpha = 12$ (left) and the absolute value of the radial dependence of its Fourier transform (right)

inversion problem that is ill-posed (in the sense of Hadamard), such as the inversion of the x-ray and Radon transforms (see Chapter 4 of Natterer & Wübbeling (2001)), such a constraint act to regularise the iterative solution. In particular, for the smoothness assumption suppresses the recovery in inversion of *ghosts*, functions in the null-space of the corresponding finite-data transform (see Louis (1984)). Noting that the usual pixel representation (i. e., with respect to a basis of characteristic functions of pixels) has a slow decay in the Fourier transform of its basis, Lewitt proposes representation with respect to a basis of translates of a single, radially symmetric, function

$$b_i(\mathbf{y}) = \Psi(\mathbf{y} - \mathbf{y}_i) = \psi(\|\mathbf{y} - \mathbf{y}_i\|),$$

whose *window* function, ψ, is a generalisation of the Kaiser-Bessel window used in signal processing (and reduces to it for $m = 0$)

$$\psi(r) = \begin{cases} (1 - (r/a)^2)^{m/2} I_m(\alpha\sqrt{1 - (r/a)^2})/I_m(\alpha) & (r < a) \\ 0 & \text{otherwise} \end{cases}, \tag{3.12}$$

where I_m is the modified Bessel function of order m, as in Watson (1944).

In (3.12), the parameter a is the radius of the support of Ψ, α controls the localisation of Ψ about zero, while m determines its smoothness of $\Psi(\mathbf{y})$ for $\|\mathbf{y}\| = a$. An example of the basis function in dimension two is shown in Figure 6, and one can see the reason for Lewitt's choice of the nickname "blobs" for these functions.

Lewitt's basis functions possess a number of attractive features, both theoretically and computationally:

- The radial dependence of the Fourier transform $\hat{\Psi}(\|\mathbf{y}\|)$ (calculated explicitly in Lewitt (1990)) has asymptotic decay $O(1/\|\mathbf{y}\|^{m+1})$, and thus the degree of localisation of the Fourier transform about zero can be controlled by a single parameter;
- A number of interesting quantities associated with Ψ: its gradient, Fourier transform and Laplacian, may be calculated explicitly. In particular the projection p of Ψ, i. e., the integral over the line whose closest point to zero is a distance s from it, is

$$p(s) = 2\int_o^\infty \psi_m(\sqrt{s^2 + t^2})\,\mathrm{d}t = a\frac{I_{m+1/2}(\alpha)}{I_m(\alpha)}\left(\frac{2\pi}{\alpha}\right)^{1/2}\psi_{m+1/2}(s) \tag{3.13}$$

where the dependence of ψ on m is here indicated by its subscript;

- The freedom in the choice of the parameters may be used to ensure that the resulting basis has desirable properties (a small error in representing constant functions, invertib-

ility of the interpolation matrix $[\Psi(\mathbf{y}_i - \mathbf{y}_j)]$ and so on). These matters are discussed in Matej (1996) and Green (2001);

• The modified Bessel function I_ν can be calculated simply and efficiently for ν a half-integer, as is described in Thompson (1997).

A systematic evaluation of the application of Lewitt's basis for a number of inversion methods (including ART) in positron emission tomography has found a clear advantage over pixel (or voxel) based discretisations (see Matej *et al.* (1994)). It is our hope that these benefits will transfer to the discretisation of Barrick's equation.

Implementation for Barrick's equation

The combination of Lewitt's basis with the discretisation of Barrick's equation (3.5) is achieved simply by substituting the expression for the projection of Lewitt's basis (3.13) into that for the localised projection (3.9). Thus the coefficients $B_{i,j}$ can be obtained by the following procedure applied for each grid-node $\mathbf{y}_i$ and for each chosen sideband (i. e., for each of the corresponding choices of m and m'):

- calculate $\frac{\partial \xi}{\partial y}(\mathbf{y}_i)$ and $|\nabla \xi|\,(\mathbf{y}_i)$ using (3.11);
- calculate the integration limits $s_{i,j}$ from (3.10);
- for each pair $(s_{i,j}, s_{i,j+1})$:
  - calculate the strip-integral approximation (3.9) using the formula (3.13);
  - evaluate $B_{i,j}$ from (3.6).

The main computational cost in this procedure is the (numerical) integration of the projection p of the basis function, but this can be greatly reduced by creating an appropriate approximation of the indefinite integral.

For practical discretisation a number of minor complications, ignored in the above for the sake of brevity, must be incorporated in the calculations.

For Doppler spectra obtained from shallow-water observations, the formulae for the kernel and integration contours need to be modified to account for the shallow-water dispersion relation. Details on the required changes can be found in Holden & Wyatt (1992).

Combining the discretisations for multiple radar systems may present a problem if the radars are operating at different frequencies, for then the y variables from the discretisations are incommensurate. This is solved by a suitable scaling, but then one might as well discretise in the k domains, and perform the normalisation as required (or use the corresponding unnormalised formulae).

Finally, the $\mathbf{y}$ domain as described above is rather narrow (see Figure 4), so discretisation with a basis function whose support is a disc leads to undersampling in the y variable (or oversampling in angle). Consequently, a scaling of the y variable (as mentioned in Lewitt (1990)) is needed, forcing a few trivial modifications.

Review of discretisation methods

We here provide a brief overview of some of the discretisation schemes that have been used in the inversion of Barrick's equation.

The first inversion method, described in Lipa (1977), makes reductions in the complexity of the inversion by assuming that the directional spectrum is separable, $S(\mathbf{k}) = g(k)h(\theta)$. Such an assumption, often reasonable, allows the separation of the discretisation and reduces the number of unknowns to such an extent that the resulting linear system is overdetermined.

The discretisation adopted by Lipa & Barrick (1980), and later by Howell & Walsh (1993), replaces separability by the less restrictive assumption that the direction spectrum

is well approximated by a truncated Fourier series in angle

$$S(\mathbf{k}) = \sum_{n=1}^{N} (a_n(k) \cos n\theta + b_n(k) \sin n\theta).$$

As with Lipa's approach, this leads to a lightweight discretisation since only the $2N$ one-dimensional functions a_n and b_n need be determined, and satisfactory results are reported for $N = 2$ or 3.

The inversion method of Wyatt (1990), a two-dimensional version of the iterative scheme described in § 7.6 of Twomey (1977), is rather unusual in that the discretisation of the directional spectrum is along the contours of integration defined by the Dirac constraint (as in Figure 4). This approach has the advantage that the solution to the forward problem (needed in each iteration) is rapid, albeit at the expense of finding nearest-neighbours for each discretisation point, needed for the smoothing which stabilises the inversion.

Finally we mention the more traditional grid-based discretisations associated with the nonlinear inversion method of Hisaki (1996), and the Bayesian inversion of Hashimoto & Tokuda (1999). These authors represent the directional spectrum as piecewise-constant on pixels which are uniform in θ, but exponential in wavenumber.

4. Preliminary results

The discretisation described above has been implemented as part of an experimental replacement inversion kernel for the Sheffield wave inversion toolset. The toolset implements the results of research into the inversion problem by L. R. Wyatt and co-workers over 15 years (Holden & Wyatt (1992), Wyatt (1986), Wyatt (1990), Wyatt, Ledgard & Anderson (1997)), and was recently deployed as part of the EuroROSE project described in Wyatt *et al.*.

An important design goal for the implementation was modularity, since we wish the discretisation to be usable with any inversion method which can be recast as a row-action method (in particular with Wyatt's inversion method). The discretisation, generic row-action method and ART modules were implemented in around 20,000 lines of C, chosen for reasons of efficiency and portability. The initial implementation was found to have a performance close to that of the (highly optimised) Wyatt algorithm used in the EuroROSE project, with an inversion performed in an amortised half-second on a 750MHz PIII, around four times as fast as was needed for real-time operation during EuroROSE (where 200–350 inversions were performed every 10 minutes).

Figure 7 shows an example of inversion of data acquired during the EuroROSE Fedje deployment. A pair of Doppler spectra (right, in grey) were inverted using the ART, with 25 iterations and a relaxation parameter of 0.1. The discretisation for the inversion used the radial Lewitt basis arranged on a regular 64×30 cylindrical grid in the y-θ domain. The directional spectrum (left) is dominated by low frequency waves at around 0.1 Hz heading south eastward, typical for the exposed location. The estimate of the Doppler spectra derived from the directional spectrum *via* Barrick's second-order equation, which drive the inversion, is shown superimposed (in black) on the measured Doppler spectra (left).

A detailed comparison of row-action methods for use with our discretisation will be reported elsewhere.

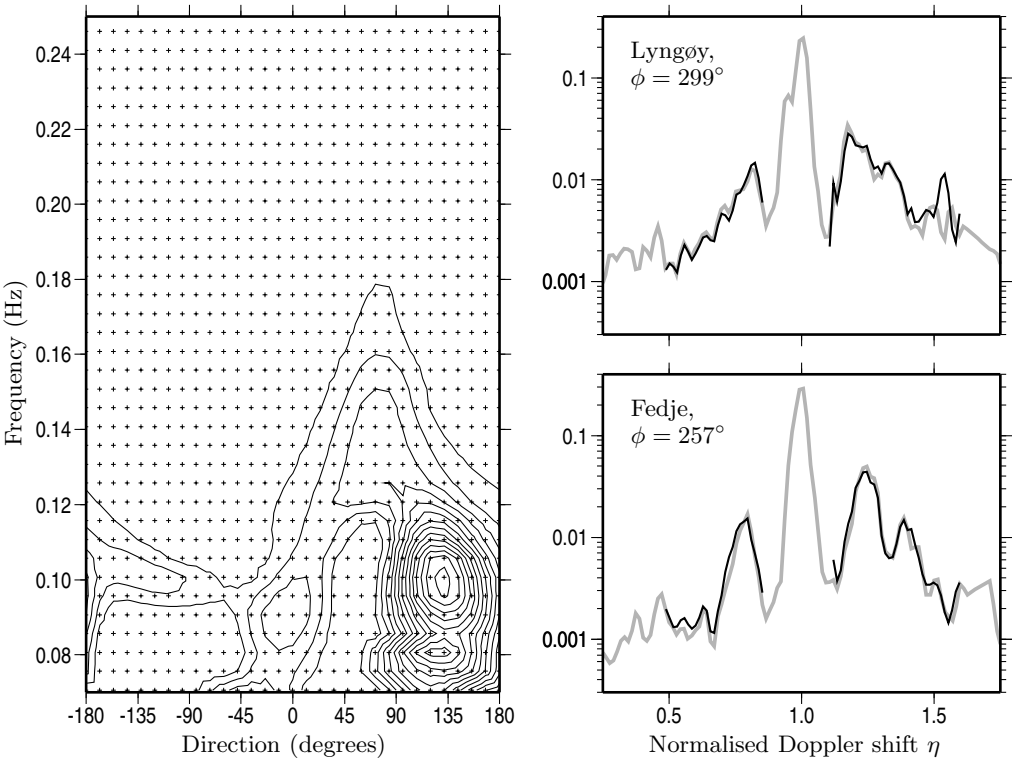

FIGURE 7. Sample directional spectrum (left) as inverted from measured Doppler spectra, detail around the positive Bragg peak shown in grey (right).

Acknowledgements

The author wishes to thank L. R. Wyatt for support and advice on the research leading to this article, and acknowledges the financial support provided through the EUROROSE project (EU contract MAS3CT980168).

REFERENCES

BARRICK, D. E. 1972 First-order theory and analysis of MF/HF/VHF scatter from the sea. *IEEE Trans. Antennas Propogat.* **AP-20**, 2–10.

BARRICK, D. E. & LIPA, B. J. 1986 The second-order shallow-water hydrodynamic coupling coefficient in interpretation of HF radar sea echo. *IEEE J. Oceanic Eng.* **OE-11 (2)**, 310–315.

BARRICK, D. E. & WEBER, B. L. 1977 On the nonlinear theory for gravity waves on the ocean's surface. Part II: Interpretation and applications. *J. Phys. Oceanog.* **7**, 11–21.

CENSOR, Y. 1981 Row-action methods for huge and sparse systems and their applications. *SIAM Review* **23 (4)**, 444–466.

FLEMING, H. E. 1980 Equivalence of regularization and truncated iteration in the solution of ill-posed image reconstruction problems. *Linear Alg. Applic.* **130**, 133–150.

GORDON, R., BENDER, R. & HERMANN, G. T. 1970 Algebraic reconstruction techniques (ART) for three-dimensional electron microscopy and x-ray photography. *J. Theoret. Biol.* **29**, 471–481.

GREEN, J. J. 2001 Approximation with the radial basis functions of Lewitt. To appear in *Proceedings of Algorithms for Approximation 4*.

Hashimoto, N. & Tokuda, M. A Bayesian approach for estimating directional spectra with HF radar. *Coastal Eng. J.* **41 (2)**, 137–149.

Helgason, S. 1999 *The Radon transform.* Progress in Mathematics, vol. 5, Birkhäuser.

Hisaki, Y. 1996 Nonlinear inversion of the integral equation to estimate ocean wave spectra from HF radar. *Radio Science* **31 (1)**, 25–39.

Holden, G. J. & Wyatt, L. R. 1992 Extraction of sea state in shallow-water using HF radar. *IEE Proc. F Radar Sig. Proc.* **139**, 175–181.

Hounsfield, G. N. 1973 Computerized transverse axial scanning (tomography), I: Description of system. *Brit. J. Radiol.* **46**, 1016–1022.

Howell, R. & Walsh, J. 1993 Measurement of ocean wave spectra using narrow-beam HF radar. *IEEE J. Oceanic Eng.* **18**, 296–305.

Lewitt, R. M. 1990 Multidimensional digital image representations using generalized Kaiser-Bessel window functions. *J. Opt. Soc. Am. A* **7 (10)**, 1834–1846.

Lipa, B. 1977 Derivation of directional ocean-wave spectra by integral inversion of second-order radar echos. *Radio Science* **12 (3)**, 425–434.

Lipa, B. & Barrick, D. 1980 Methods for the extraction of long-period ocean-wave parameters from narrow beam HF radar sea-echo. *Radio Science* **15 (4)**, 843–853.

Louis, A. K 1984 Orthogonal function series expansion and the null space of the Radon transform. *SIAM J. Math. Anal.* **15 (3)**, 621–633.

Matej, S., Herman, G. T., Narayan, T. K., Furuie, S. S., Lewitt, R. M. & Kinahan, P. E. 1994 Evaluation of task-oriented performance of several fully 3d PET reconstruction algorithms. *Phys. Med. Biol.* **39**, 355–367.

Matej, S. & Lewitt, R. M. 1996 Practical considerations for 3-d image reconstructions using spherically symmetric volume elements. *IEEE Transactions on Medical Imaging* **15 (1)**, 68–78.

Natterer, F. & Wübbeling, F. 2001 *Mathematical Methods in Image Reconstruction* SIAM Monographs on Mathematical Modeling and Computation, vol. 5, SIAM.

Pierson Jr, W. J. & Moskowitz, L. 1964 A proposed spectral form for fully developed wind seas based on the similarity theory of S. A. Kitaigorodskii. *J. Geophys. Res.*, 5181–5190.

Thompson, W. J. 1997 *Atlas for computing mathematical functions.* John Wiley & Sons Inc.

Twomey, S. 1977 *Introduction to the Mathematics of Inversion in Remote Sensing and Indirect Measurements.* Dover.

Watson, G. N. 1944 *A Treatise on the Theory of Bessel Functions*. Cambridge.

Weber, B. L. & Barrick, D. E. 1977 On the nonlinear theory for gravity waves on the ocean's surface. Part I: Derivations. *J. Phys. Oceanog.* **7**, 3–10.

Wyatt, L. R. 1986 The measurement of the ocean wave directional spectrum from H.F. radar Doppler spectra. *Radio Science* **21**, 473–485.

Wyatt, L. R. 1990 A relaxation method for integral inversion applied to HF radar measurement of the ocean wave directional spectrum. *Int. J. Remote Sensing* **11**, 1481–1494.

Wyatt, L, R., Green, J. J., Gurgel, K.-W., Nieto Borge, J. C., Reichert, K., Günther, H., Rosenthal, W., Saetra, O. & Reistad, M. (in press) Comparisons of wave measurements from the EuroROSE Fedje experiment.

Wyatt, L. R., Ledgard, L. J. & Anderson, C. W. 1997 Maximum-likelihood estimation of the directional distribution of 0.53-Hz ocean waves. *J. Atmos. Oceanic Tech.* **14**, 591–603.